Intratumoral and peritumoral radiomics of MRI predict pathological differentiation in patients with rectal cancer

HUANHUI LIU, HANJING ZHANG, QIAN ZOU and JIANQUAN YANG

Department of Oncology, Affiliated Hospital of North Sichuan Medical College, Nanchong, Sichuan 637000, P.R. China

Received May 14, 2025; Accepted October 7, 2025

DOI: 10.3892/ol.2025.15363

Abstract. The histopathological differentiation of rectal cancer (RC) is a key determinant of treatment strategy and prognosis, as tumors with varying differentiation demonstrate notable differences in therapeutic approach selection and survival outcomes. Consequently, accurate preoperative prediction of tumor differentiation is clinically essential for formulating initial surgical plans and adjuvant therapy strategies. The aim of the present study was to develop a magnetic resonance imaging (MRI)-based radiomics strategy that integrates features from both intratumoral and peritumoral (margin, 5 mm) regions to construct a non-invasive predictive model capable of distinguishing well differentiated RC (glandular structures ≥95%) from non-well differentiated RC. A retrospective analysis was performed using data from 224 patients with RC who underwent preoperative MRI. Radiomic features were extracted from T1-weighted images (T1WI), T2-weighted images (T2WI) and diffusion-weighted imaging (DWI) of the tumor and peritumoral 5 mm. The adaptive synthetic technique was used to address class imbalance, and ReliefF was applied to select 20 features. A total of three machine learning algorithms, logistic regression, Light Gradient-Boosting Machine (LightGBM) classifier and Gaussian Naive Bayes, were used to build MRI radiomic models combining the tumor and the peritumoral areas to predict pathological differentiation of RC. The models were evaluated by comparing the area under the curve (AUC) and binary classification metrics, with the best performing T1-LightGBM model selected. Subsequently, intratumoral and peritumoral and intratumoral (T1-LightGBM) models were established. Discriminative ability, calibration and clinical applicability were assessed using receiver operating characteristic curves, calibration curves and decision curves, with Shapley Additive explanations (SHAP) analysis employed for interpretation. Among the nine models constructed using T1WI, T2WI and DWI from the tumor and 5-mm surrounding region, the AUC range was 0.510-0.756 across all validation sets. The T1-LightGBM model incorporating both tumor and peritumoral areas demonstrated the best performance for predicting pathological differentiation in RC, with an AUC of 0.756, accuracy of 0.700 and sensitivity of 0.707. SHAP analysis identified wavelet_HHH_glszm_Size_Zone_Non_Uniformity_Normalized as the most significant feature for predicting pathological differentiation and evaluating non-well differentiated patients. In conclusion, the integrated model employing the LightGBM algorithm on T1WI, which combined both intratumoral and 5-mm peritumoral features, demonstrated promising predictive potential for individualized RC differentiation.

Introduction

Colorectal cancer is the third most common cancer globally and the second leading cause of cancer-related deaths (1). According to the World Health Organization (WHO) classification of tumors of the digestive system (2), rectal cancer (RC) can be histologically graded as well differentiated, moderately differentiated, poorly differentiated and undifferentiated. Different histopathological grades markedly influence treatment strategies and prognosis (3). For patients with early local tumor-stage RC and no lymph node or distant metastasis (cT1N0M0), survival rates are relatively high following endoscopic resection, local excision or segmental resection, with chemotherapy not typically required postoperatively (4). However, if post-endoscopic resection pathology reveals high-risk recurrence factors, such as moderate-to-poor differentiation, vascular invasion or positive resection margins, clinical guidelines recommend additional segmental resection and regional lymph node dissection (5). For rectal adenocarcinoma with moderate differentiation and late-stage local tumor (T)-stage such as T4a and T4b, local excision is prone to residual cancer, and neoadjuvant therapy followed by radical total mesorectal excision surgery is recommended (6). Poorly differentiated or undifferentiated carcinomas indicate more aggressive tumor biology, with a higher likelihood of early metastasis and worse prognosis (7). These cases often necessitate more aggressive treatment approaches which may include additional surgical resection of the primary lesion and regional lymphadenectomy. Postoperative adjuvant radiotherapy or

Correspondence to: Professor Jianquan Yang, Department of Oncology, Affiliated Hospital of North Sichuan Medical College, 1 Maoyuan South Road, Nanchong, Sichuan 637000, P.R. China
E-mail: nscmcphdcyjq@163.com

Key words: rectal cancer, machine learning, radiomics, pathological differentiation, peritumoral

chemotherapy is often required to improve overall therapeutic efficacy. Notable, the outcomes of salvage surgery for patients with recurrence after local excision are limited. The 3-year overall survival rate is only ~31, and ~39% of patients develop distant metastases (8). However, Hahnloser *et al* (9) reported that, when extended resection was performed within 30 days of local excision, the 5-year survival rate was comparable with that of patients who initially underwent radical resection. Therefore, if the initial pathology following local excision indicates poor differentiation, interval radical resection should be considered. Nevertheless, this approach may compromise sphincter preservation, leading certain patients to opt for adjuvant chemoradiotherapy instead (10). In summary, accurate preoperative prediction of the histological differentiation of RC is of paramount importance, as it directly influences surgical recommendations and patient decision-making prior to the initial intervention.

Magnetic resonance imaging (MRI) is essential for the non-invasive characterization of RC, providing superior soft tissue resolution and offering more accurate insights into the heterogeneity of the tumor compared with other imaging modalities (11). However, pathological differentiation is still primarily dependent on postoperative pathological biopsy (12), and there is insufficient evidence to demonstrate that conventional imaging techniques can reliably differentiate pathological grading of RC. Consequently, there is a pressing need for more intelligent and sensitive diagnostic technologies to enable preoperative assessment of RC differentiation. Radiomics, which extracts numerous quantitative features from medical images, has shown notable potential in evaluating RC characteristics (13). Existing studies have indicated that radiomic features based on MRI of the primary tumor can predict the pathological differentiation of other tumors. However, most of these studies have focused primarily on the intratumoral features (14,15), neglecting potentially valuable information in the peritumoral region and requiring more clinical interpretability which hinders the widespread application of imaging models.

The peritumoral region includes endothelial cells, fibroblasts, immune cells, other cell types and extracellular components, forming the tumor microenvironment (16). The tumor microenvironment serves a decisive role in tumor progression, treatment response and metastasis. Therefore, radiomic features of the peritumoral environment may provide crucial data for clinically assessing the aggressive biological behavior of tumors. Whilst Liu *et al* (17) reported that peritumoral tissues in hepatocellular carcinoma (HCC) are associated with pathological differentiation, systematic exploration of the relationship between peritumoral tissues and pathological differentiation in patients with RC is lacking, and the value of peritumoral features in predicting RC pathological differentiation remains controversial.

Therefore, the aim of the present study was to construct a predictive model based on intratumoral and peritumoral (within 5 mm of the tumor) radiomics features derived from multiparametric MRI to achieve preoperative noninvasive differentiation between well differentiated RC (adenomatous structure ≥95%) and non-well differentiated RC. Furthermore, a preoperative radiomics model that integrates the optimal features from both intratumoral and 5-mm peritumoral regions was developed and validated, with the goal of providing an imaging-based reference for accurate preoperative assessment and clinical decision-making in RC.

Materials and methods

Patient selection. The Medical Ethics Committee of the Affiliated Hospital of North Sichuan Medical College (Nanchong, China) approved the current retrospective study (approval no. 2024ER490-1) and waived the requirement for informed consent from patients. The data of 224 patients with RC who underwent surgery between January 2017 and February 2024 at the Affiliated Hospital of North Sichuan Medical College were retrospectively analyzed. All patients underwent preoperative MRI scanning, and the diagnosis of adenocarcinoma was confirmed by pathological examination after surgery.

The inclusion criteria were as follows: i) Primary RC; ii) pathologically-confirmed adenocarcinoma; iii) postoperative pathological findings with clear pathological differentiation; iv) lesions which could be identified on MRI images and could be successfully enlarged peritumorally; v) no radiotherapy prior to surgery; and vi) radical, endoscopic resection or palliative resection. The exclusion criteria were as follows: i) Lack of description or formal report regarding the degree of tumor differentiation (n=13); ii) incomplete MRI sequences or poor image quality (n=31); iii) previous history of other tumors in combination (n=6); and iv) pathological diagnosis of squamous, carcinoid and neuroendocrine tumors (n=27). After appropriate screening, a total of 224 patients were included in the present study, who were randomized into training or validation groups in a ratio of 7:3.

Pathological differentiation analysis. Tumor specimens underwent hematoxylin and eosin (HE) staining in the Department of Pathology at the Affiliated Hospital of North Sichuan Medical College to determine the degree of differentiation in RC. The samples were fixed with 4% paraformaldehyde at 20-25˚C for 24 to 48 h, followed by dehydration, paraffin infiltration, embedding, and sectioning to a thickness of 4-6 μm. Prior to HE staining, the sections are baked at 60-65˚C for 1 h, then subjected to deparaffinization using a graded ethanol series and xylene, followed by rehydration. The sections are subsequently stained with hematoxylin for 3-5 min and counterstained with eosin for 1-3 min at room temperature. After staining, the sections are dehydrated through a graded alcohol series, cleared with xylene, and finally mounted with neutral gum. The prepared samples can be observed for morphological analysis under a light microscope. According to classification standards (2), RC tumors were classified as one of the following: i) Well differentiated, (grade 1), glandular ductal structures account for >95% of the tumor; ii) moderately differentiated (grade 2), glandular ductal structures account for 50-95% of the tumor; iii) poorly differentiated (grade 3), glandular ductal structures account for 5-50% of the tumor; or iv) undifferentiated (grade 4), not obvious undifferentiated features and proportion of glandular ducts accounts for <5% of the tumor. The latter category encompasses mucinous adenocarcinomas and impression cell carcinomas. When RC tumors demonstrated different differentiation results, the

predominant differentiation determined the final diagnosis. RC was classified according to the degree of differentiation into well differentiated and non-well differentiated.

MRI protocol. All patients with RC underwent MRI using a MAGNETOM Skyra 3.0T (Siemens Healthineers) scanner prior to surgery. Patients fasted for 4-6 h before the examination and underwent bowel preparation 2 h before the scan. An abdominal phased-array coil was used. Scanning sequences included T1_tse_tra, t2_blade_tra_p2_320 and ep2d_diff_tra_b50-1000_TRACEW_DFC_MIX. The specific parameters used were as follows: i) T1_tse_tra: Repetition time (TR) of 613 msec, Echo time (TE) of 10 msec, inversion angle of 160˚, slice thickness of 3.5 mm, interslice distance of 3.85 mm, matrix of 320x288, Field-of-view (FOV) of 190x190 mm and voxel size of 0.6x0.6x3.5 mm; ii) T2_blade_tra_p2_320: TR of 5,010 msec, TE of 87 msec, inversion angle of 160˚, slice thickness of 3.5 mm, interslice distance of 3.85 mm, matrix of 320x320, FOV of 190x190 mm and voxel size of 0.6x0.6x3.5 mm; and iii) ep2d_diff_tra_b50-1000_TRACEW_DFC_MIX: TR of 5,400 msec, TE of 75 msec, inversion angle of 90˚, slice thickness of 3.5 mm, interslice distance of 3.85 mm, matrix of 150x142, FOV of 301x301 mm, voxel size of 2.0x2.1x3.5 mm and b-values of 50 and 1,000 s/mm^2.

Data collection. The data collected included age, sex, carcinoembryonic antigen (CEA), carbohydrate antigen 19-9 (CA 19-9), aspartate aminotransferase (AST), prealbumin, albumin-to-globulin ratio, total bilirubin, direct bilirubin, lactate, creatinine, leucine aminopeptidase, γ-glutamyl transferase, adenosine deaminase, alkaline phosphatase, white blood cells, red blood cells, serum albumin, hemoglobin, platelets, neutrophils, lymphocytes, monocytes and the hemoglobin, albumin, lymphocyte, and platelet score, all within 2 weeks before surgery. Pathological data included differentiation grade, whilst imaging data included the distance of the tumor from the anal verge, lesion length, tumor-node-metastasis (TNM) stage, circumferential resection margin (CRM) and extramural vascular invasion.

Imaging preprocessing, region of interest (ROI) segmentation and peritumoral region dilation. Images were resampled at a voxel spacing of 1x1x1 mm^3 before delineating the ROI and normalizing to grayscale to compensate for voxel spatial differences and maintain grayscale consistency, respectively. The entire ROI of T1-weighted images (T1WI), T2-weighted images (T2WI) and diffusion-weighted imaging (DWI) was outlined by a senior radiologist experienced in diagnostic imaging of RC using open-source 3Dslicer software (version 5.3.0; download.slicer.org/). Furthermore, and the entire ROI of T1WI, T2WI and DWI was automatically analyzed using the 'Margin' module, which was used to automatically expand the 5-mm region around the tumor to obtain a 3D segmented image.

Feature extraction. The image and the outlined ROI structure were imported into 3D Slicer for feature extraction. The features extracted by 3D Slicer were mainly performed using the open-source plug-in (Pyradiomics v2.2.0; https://github.com/Radiomics/SlicerRadiomics). The extracted features included mean, minimum, maximum, standard deviation, skewness, kurtosis and others of the first-order statistical features of the original image, as well as the surface area, volume, surface area-to-volume ratio, sphericity, compactness and 3D diameter of the morphological features. Moreover, the following five types of texture features were extracted (18): i) Gray Level Cooccurence Matrix; ii) Gray Level Run Length Matrix; iii) Gray Level Size Zone Matrix; iv) Neighbouring Gray Tone Difference Matrix; and v) Gray Level Dependence Matrix. Shape features were extracted from the original images, while first-order and texture features were obtained from both the original images and their filtered versions. The filtering procedures included: Wavelet transformation (utilizing high-pass (H) and low-pass (L) filters along the x, y, and z axes, generating eight distinct decomposition combinations: HHH, HHL, HLH, LHH, LLL, LLH, LHL, HLL) and Laplacian of Gaussian (LoG) filtering (σ=4.0, 5.0, and 6.0 mm). In this case, the wavelet transform image was created using the default parameters of 3D Slicer. The wavelet sequence used was Daubechies (Db4). A 3-layer decomposition was performed. The fill mode was symmetric filling. Quantization of 64 bins was applied. The sampling mode was custom sampling, with specific sampling densities of x-, y- and z-axis sampling intervals of 4, 5 and 6 voxels, respectively. A total of 1,223 features were extracted.

Imbalanced data processing. The dataset comprised 46 patients with well differentiated tumors and 178 with non-well differentiated tumors. However, the marked imbalance between the two groups could impair classifier performance; therefore, to address this, the adaptive synthetic (ADASYN) technique was employed to balance the dataset (19). After resampling, the proportion of well differentiated and non-well differentiated cases reached 1:1, with the minority class increasing from 20.5% in the original dataset to 50.8% after ADASYN processing. Specifically, the number of patients with well differentiated and non-well differentiated tumors was 184 and 178, respectively. Subsequently, ReliefF (20) was used for dimensionality reduction, selecting 20 notable distinguishing features. The balanced dataset was randomly divided into a training set (70%) and a testing set (30%) after five-fold cross-validation.

Establishment and evaluation of the predictive model. In the current study, three machine learning algorithms, logistic regression, Light Gradient Boosting Machine (LightGBM) Classifier and Gaussian Naive Bayes, were selected to predict the pathological differentiation of patients with RC based on imaging features in and around the 5-mm region of the tumor in T1WI, T2WI and DWI. The model was constructed using k-fold cross-validation on the training set as a resampling method (k=5) and the hyperparameters were adjusted using grid search to build the best model using the optimal parameters. The receiver operating characteristic (ROC) curve was plotted with the true positive rate as the vertical coordinate and the false positive rate as the horizontal coordinate, and the predictive efficacy of the model was evaluated by calculating the area under the receiver operating curve (AUC) and validated in the test group. The accuracy, sensitivity and specificity corresponding to the optimal thresholds of each model

Table I. Evaluation of the performance of classification models on imbalance dataset using the adaptive synthetic technique in the validation set.

Model	AUC (SD)	Accuracy (SD)	Sensitivity (SD)	Specificity (SD)	PPV(SD)	NPV (SD)	F1 score (SD)	Cutoff (SD)
Logistic								
T1WI	0.637 (0.056)	0.542 (0.039)	0.552 (0.134)	0.512 (0.145)	0.591 (0.037)	0.474 (0.089)	0.563 (0.084)	0.445 (0.045)
T2WI	0.533 (0.104)	0.521 (0.100)	0.184 (0.121)	0.799 (0.256)	0.600 (0.261)	0.535 (0.086)	0.229 (0.106)	0.544 (0.006)
DWI	0.615 (0.079)	0.568 (0.046)	0.291 (0.176)	0.779 (0.170)	0.558 (0.176)	0.556 (0.060)	0.356 (0.169)	0.556 (0.072)
LightGBM								
T1WI	0.756 (0.051)	0.700 (0.074)	0.707 (0.122)	0.700 (0.204)	0.730 (0.140)	0.709 (0.053)	0.700 (0.070)	0.452 (0.291)
T2WI	0.601 (0.096)	0.561 (0.098)	0.536 (0.234)	0.628 (0.163)	0.578 (0.079)	0.598 (0.162)	0.521 (0.130)	0.668 (0.260)
DWI	0.750 (0.073)	0.658 (0.080)	0.600 (0.258)	0.704 (0.292)	0.763 (0.160)	0.646 (0.130)	0.608 (0.142)	0.380 (0.194)
GNB								
T1WI	0.672 (0.107)	0.621 (0.094)	0.856 (0.056)	0.421 (0.181)	0.591 (0.130)	0.741 (0.098)	0.687 (0.074)	0.001 (0.002)
T2WI	0.501 (0.108)	0.471 (0.068)	0.293 (0.131)	0.668 (0.251)	0.552 (0.255)	0.493 (0.040)	0.324 (0.099)	0.107 (0.032)
DWI	0.645 (0.085)	0.579 (0.076)	0.540 (0.160)	0.620 (0.150)	0.587 (0.050)	0.585 (0.150)	0.546 (0.081)	0.039 (0.027)

AUC, area under the curve; SD, standard deviation; PPV, positive predictive value; NPV, negative predictive value; WI, weighted image; DWI, diffusion-weighted imaging; LightGBM, Light Gradient Boosting Machine; GNB, Gaussian Naive Bayes.

were obtained by selecting the optimal thresholds based on the Youden index. Confusion matrix metrics, such as AUC, accuracy, sensitivity, specificity and F1 score, were used to evaluate the prediction performance and stability of each model. Following the identification of the optimal classification method and imaging sequence for predicting the pathological differentiation of RC through comparison with confusion matrix metrics and standard deviations derived from forest plots, the dataset was re-divided into a training set (70%), a validation set (15%) and a test set (15%). The validation set was used to adjust the model parameters and the test set was used to evaluate the system performance. T1-LightGBM models of intratumor and intratumor + peritumor were constructed, and then ROC curves, learning curves, calibration plots and decision curve analysis (DCA) were used to further assess the clinical efficacy of the prediction models. Calibration curves reflect how well the predicted probability matches the actual outcome; DCA was used to assess the net benefit of the model at different thresholds. Calibration was assessed using the Hosmer-Lemeshow goodness-of-fit test, followed by development of the Shapley Additive explanations (SHAP) overall presentation model and single-sample interpretation.

Statistical analysis. Categorical data are presented as n (%), whilst continuous variables are expressed as median (interquartile range). Differences between well differentiated and non-well differentiated groups were assessed using the Wilcoxon rank sum test, Fisher's exact test or Pearson's χ^2 test. A two-sided $P<0.05$ was considered to indicate a statistically significant difference. Statistical analyses were performed using R 3.6.3 (https://www.r-project.org/) and Anaconda Python 3.7 (anaconda.com/).

Results

Patient characteristics. Postoperative pathological reports categorized the 224 patients into the well differentiated group (n=46) and the non-well differentiated group (n=178). Baseline patient data are presented in Table SI. CA 19-9, AST and alanine aminotransferase were significantly associated with pathological tissue differentiation ($P<0.05$), whilst no significant differences were observed in other clinical indicators or characteristics.

Feature analysis. A total of 1,224 features were extracted and standardized. Table I presents the application results of machine learning classification algorithms on the balanced dataset generated using ADASYN. The T1-LightGBM model demonstrated the best performance in the validation set.

Model development and evaluation. A total of three machine learning algorithms were used to develop predictive models. Fig. 1 illustrates the ROC curves for the different models constructed for the intratumoral + peritumoral features. The AUC range for the models was 0.510-0.756 across all validation cohorts. The T1-LightGBM model, which combined intratumoral and peritumoral features, achieved AUC, accuracy, sensitivity, positive predictive value (PPV), negative predictive value (NPV) and F1 score >0.7 in the validation set, outperforming the other eight models (Table I). Moreover,

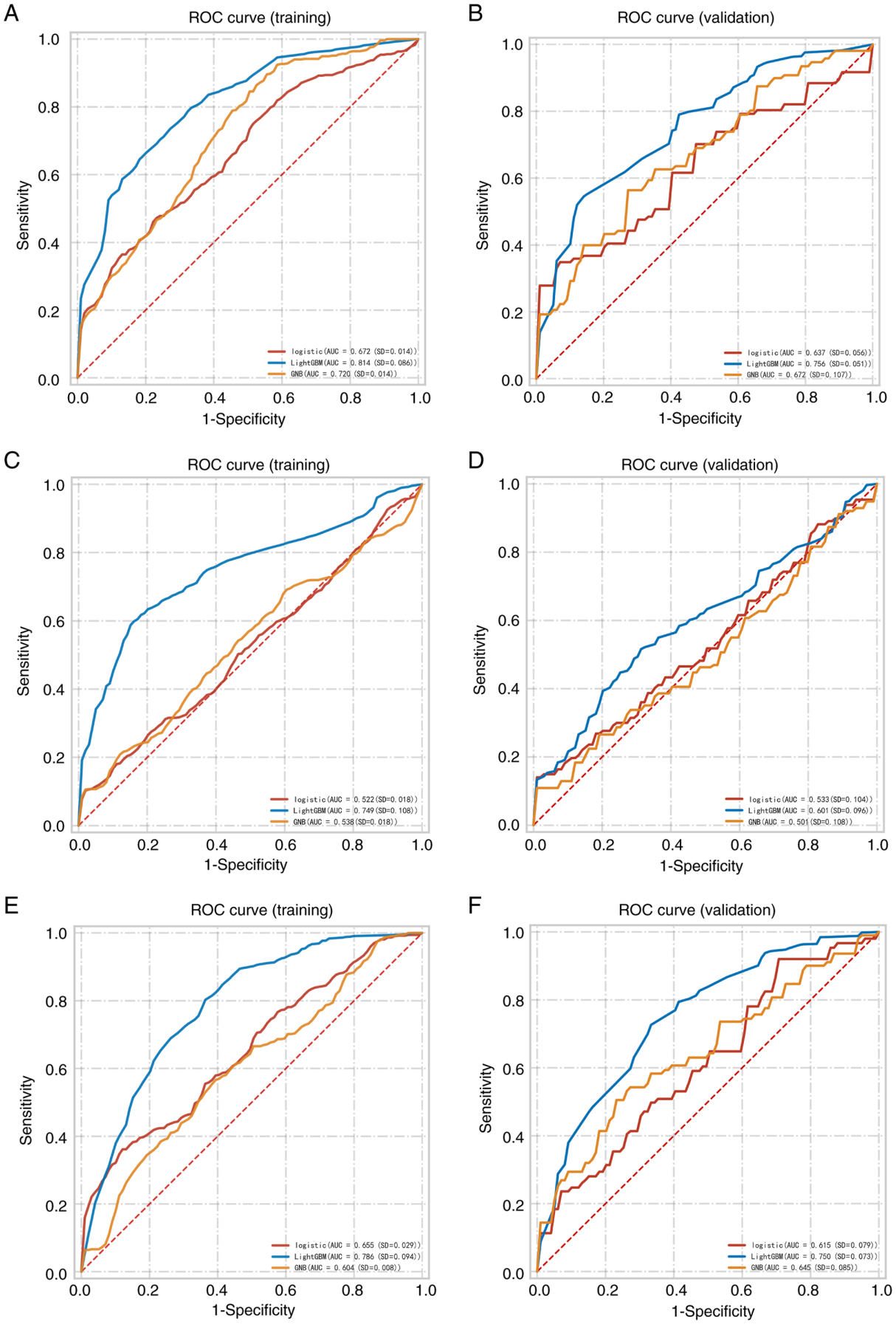

Figure 1. ROC curves for the peritumoral + intratumoral prediction model for pathological differentiation of rectal cancer. ROC (A) training and (B) validation curves for T1WI imaging. ROC (C) training and (D) validation curves for T2WI imaging. ROC (E) training and (F) validation curves for diffusion-weighted imaging. ROC, receiver operating characteristic; WI, weighted image; AUC, area under the curve; LightGBM, Light Gradient Boosting Machine; GNB, Gaussian Naive Bayes.

the T1-LightGBM model demonstrated the best predictive performance on both training and validation sets (Fig. 1). The forest plot in Fig. S1 presents the ROC results for the nine models in predicting pathological differentiation, indicating that the T1-LightGBM model had the highest central value and the shortest error bars, further confirming its superior stability.

The LightGBM model was chosen as the best model for predicting pathological differentiation, and the intratumoral + peritumoral and intratumoral prediction models of T1-LightGBM were constructed using 5-fold cross-validation. The AUC, cutoff, accuracy, sensitivity, specificity, PPV and NPV for the training, validation and test cohorts are presented in Table II, and the model ROC curves are presented in Figs. 2 and 3. Assessment of the predictive performance metrics indicated that the combined intratumoral + peritumoral model outperformed the intratumoral-only model. Specifically, the average AUC of the intratumoral + peritumoral model was 0.766 for the training set, 0.690 for the validation set and 0.620 for the test set (Fig. 2A-C; Table II), and the AUC of the training, validation and test sets eventually stabilized at ~0.70. The AUC was 0.668 in the training set, 0.701 in the validation set and 0.563 in the test set for the intratumor model (Table II; Fig. 3A-C). Learning curves (Fig. 3D) were shown prior to assessing the accuracy of the model, which indicated that the difference in error between the training and the validation sets in the intratumoral + peritumoral 5-mm model converged as the number of training samples increased. This suggests that the model was not overfitted. Subsequently, the calibration curves of the validation set were used to assess the accuracy of the model. The results revealed that the intratumoral + peritumoral 5-mm T1-LightGBM model had notable agreement with the predicted probability of observed pathological differentiation (Fig. 4A). The Hosmer-Lemeshow test demonstrated that the intratumoral + peritumoral T1-LightGBM model was well-calibrated (P=0.064). Subsequently, a DCA of the model was constructed in the study, indicating that the intratumoral + peritumoral model had a more marked net benefit than all-or-none pathological differentiation with a risk threshold of <64% (Fig. 4B). By contrast, the calibration curves and DCA of the intratumoral LightGBM model (Fig. 5) performed slightly worse than the intratumoral + peritumoral prediction model. In summary, the LightGBM model may be used for classification modeling tasks in this dataset.

Model interpretation. The present study used SHAP plots to elucidate the performance of the intratumoral + peritumoral T1-LightGBM based prediction model for pathological differentiation. Fig. S2A illustrates that the feature wavelet_HHH_glszm_Size_Zone_Non_Uniformity_Normalized was the most critical predictor for pathological differentiation. Furthermore, Fig. S2B illustrates a specific case of predicting pathological differentiation in patients with RC, where the SHAP values of features are visualized as forces that either augment or diminish the predictive assessment. The baseline was 0.740, representing the average SHAP value across all predictions. The patient falls into the 'true negative' group, with SHAP values <0.740, resulting in a predicted probability of 17.0% for well differentiated RC. Notably, the feature wavelet_HHH_glszm_Size_Zone_Non_Uniformity_Normalized has a negative (blue) value, indicating its contribution to the prediction of non-well differentiated RC in this patient.

Discussion

The present study developed and assessed multiple MRI-based radiomics models, with a particular focus on the value of peritumoral features for the preoperative, noninvasive prediction of the pathological differentiation grade of RC. The results demonstrated that the LightGBM model based on the T1-weighted sequence and combining intratumoral features with those from a 5-mm peritumoral shell, achieved the best performance. These findings suggest that peritumoral radiomic features can provide clinically meaningful additional information for assessing the differentiation of RC.

MRI serves a critical role in pre- and post-treatment evaluation of RC (21). T1WI effectively delineates anatomical structures, whilst T2WI provides high-resolution soft tissue contrast, highlighting differences in internal lesion composition. DWI, particularly at high b-values (b ≥800 sec/mm^2), is highly sensitive to Brownian motion of water molecules within viable tissues and tumors, offering insights into cellular activity. DWI also demonstrates superior sensitivity in detecting small tumor lesions and pelvic lymph nodes (22). In the present study, radiomic features were extracted from intratumoral and peritumoral regions across these three sequences. The SHAP method was employed to interpret model outputs, identifying the five most contributory features for distinguishing pathological differentiation: T1_wavelet_HHH_glszm_Size_Zone_Non_Uniformity_Normalized, original_first_order_Median, wavelet_HHH_glszm_Low_Gray_Level_Zone_Emphasis, Original_shape_Maximum_2D_Diameter_Slice and wavelet_HHH_glszm_High_Gray_Level_Zone_Emphasis. The top-ranked feature, wavelet_HHH_glszm_Size_Zone_Non_Uniformity_Normalized, quantifies gray-level intensity uniformity within tumors, reflecting spatial aggregation of high-signal regions (23). This metric may be associated with tumor angiogenesis or necrotic zone distribution (24), critical for evaluating structural complexity and homogeneity (25). Such heterogeneity aligns with the infiltrative growth patterns of malignant RC, often manifesting as non-spherical morphology (26). Collectively, these features emphasize the importance of integrating morphological, statistical and textural characteristics for comprehensive tumor characterization.

Whilst aligning with established machine learning methodologies, the novelty of the current study involves dataset construction and feature selection. Prior research predominantly focused on intratumoral regions, neglecting peritumoral contributions. However, emerging evidence has highlighted the prognostic value of peritumoral features in tumor biology, as demonstrated in soft tissue sarcoma (27), head and neck squamous cell carcinoma (28), gastric cancer (29), lung cancer (30,31) and ovarian cancer (32). For instance, Liu *et al* (17) highlighted the predictive utility of peritumoral features in HCC differentiation, whilst Barge *et al* (33) identified peritumoral texture features in T1WI as key discriminators for tumor grading. Xu *et al* (22) further reported that models

Table II. Diagnostic performance of the Light Gradient-Boosting Machine model constructed from intratumoral + peritumoral and intratumoral features in predicting pathological differentiation of rectal cancer.

Model	AUC (95% CI)	Cutoff (95% CI)	Accuracy (95% CI)	Sensitivity (95% CI)	Specificity (95% CI)	PPV (95% CI)	NPV (95% CI)	F1 score (95% CI)
Training set								
Intratumoral + peritumoral_ 5 mm	0.690 (0.553-0.827)	0.383 (0.090-0.677)	0.661 (0.631-0.691)	0.731 (0.619-0.843)	0.599 (0.491-0.706)	0.626 (0.582-0.670)	0.725 (0.661-0.790)	0.668 (0.625-0.710)
Intratumoral	0.668 (0.531-0.805)	0.408 (0.088-0.729)	0.677 (0.629-0.725)	0.593 (0.512-0.674)	0.753 (0.690-0.817)	0.692 (0.624-0.760)	0.669 (0.627-0.711)	0.668 (0.531-0.805)
Validation set								
Intratumoral + peritumoral_ 5 mm	0.766 (0.706-0.826)	0.383 (0.090-0.677)	0.749 (0.701-0.798)	0.807 (0.719-0.895)	0.698 (0.616-0.780)	0.709 (0.655-0.763)	0.809 (0.733-0.886)	0.751 (0.702-0.800)
Intratumoral	0.701 (0.636-0.767)	0.408 (0.088-0.729)	0.728 (0.681-0.776)	0.622 (0.490-0.753)	0.827 (0.768-0.886)	0.771 (0.719-0.823)	0.711 (0.650-0.772)	0.701 (0.636-0.767)
Test set								
Intratumoral + peritumoral_ 5 mm	0.620 (0.462-0.777)	0.321	0.618	0.788	0.364	0.65	0.533	0.712
Intratumoral	0.563 (0.412-0.715)	0.349	0.571	0.357	0.786	0.625	0.55	0.455

AUC, area under the curve; CI, confidence interval; PPV, positive predictive value; NPV, negative predictive value.

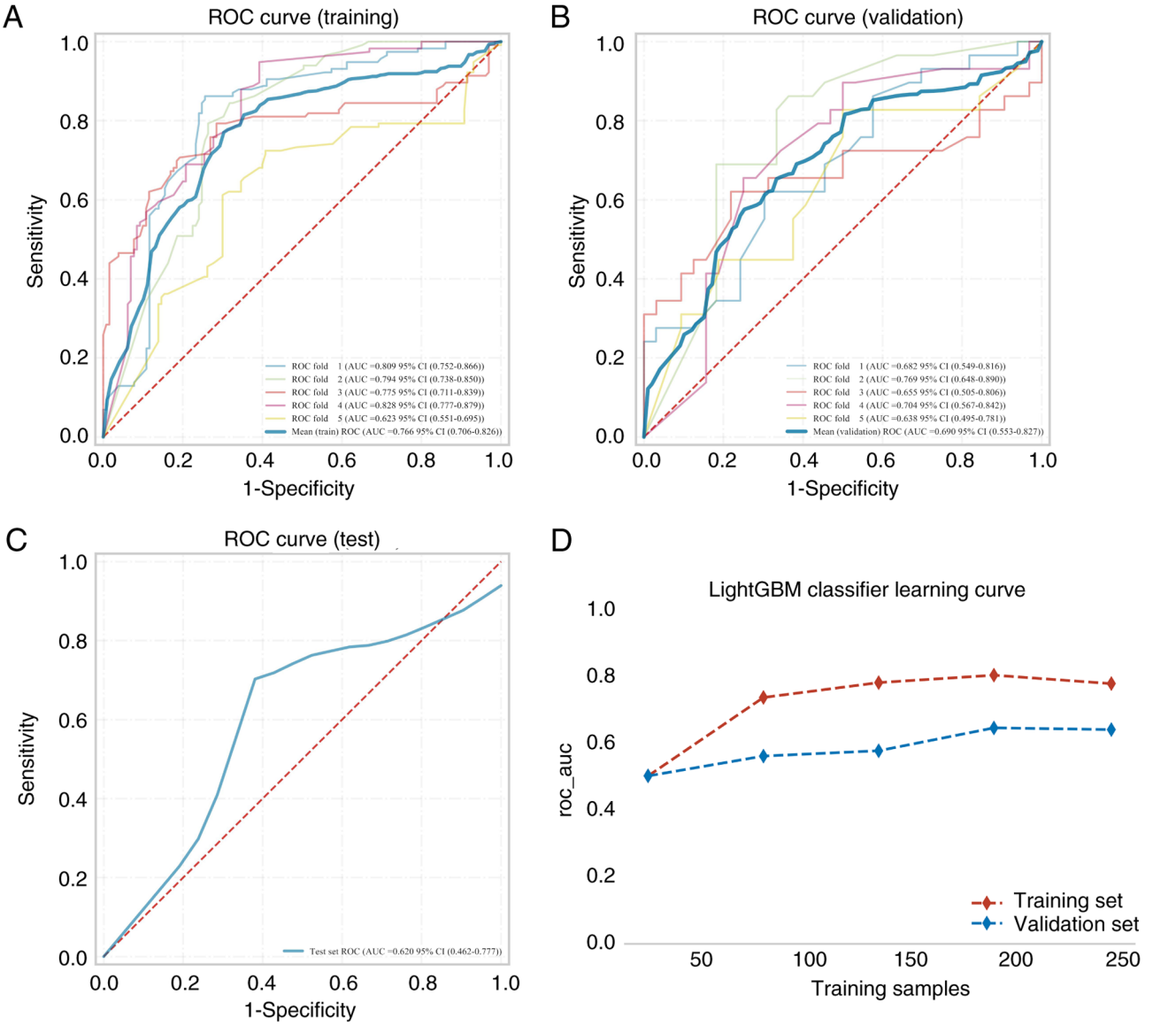

Figure 2. ROC curves of the intratumoral + peritumoral 5-mm T1-LightGBM model for the training, validation and test groups. ROC curves and AUC values for the (A) training set, (B) validation set and (C) test set. (D) Learning curves. The red dashed line represents the training set, whilst the blue dashed line represents the validation set. ROC, receiver operating characteristic; LightGBM, Light Gradient-Boosting Machine; AUC, area under the curve; CI, confidence interval.

combining intratumoral and peritumoral (3 and 5 mm) features outperformed single-region models in predicting lymphovascular invasion in RC. Based on the aforementioned rationale, the current study designated a 5-mm peritumoral region as the primary area for analysis. This choice was informed, on the one hand, by clinical consensus regarding the CRM in RC: A CRM of >1 mm is generally considered a 'safe margin' (34), although the optimal clearance remains controversial. A meta-analysis reported that, whilst a margin of >1 mm improves prognosis, a margin of >1 cm may yield superior oncological outcomes (35). On the other hand, prior peritumoral radiomics studies in lung cancer (36) and gliomas (37) suggested that regions closer to the tumor harbor richer heterogeneity; as the boundary expands outward, more normal tissue is included in the ROI, potentially diluting meaningful structural differences. Therefore, a 5-mm peritumoral band is likely to capture spatial heterogeneity whilst maximally preserving imaging signals related to tumor biology. This provides an effective basis for noninvasive, preoperative prediction of the pathological grading of RC.

Previous research has explored the relationship between functional MRI parameters and the pathological grading of RC; however, the findings have been inconsistent. Kim *et al* (38) reported that the Ktrans value in the well differentiated group in their study was significantly higher than in the moderately differentiated group (0.127±0.032 vs. 0.084±0.036; P=0.036). By contrast, Shen *et al* (39) reported that the Ktrans value was significantly associated with the pathological differentiation of RC (poor, 0.284±0.068 and moderately: 0.280±0.067 vs. well: 0.182±0.153, P=0.004), with the well differentiated group showing lower Ktrans values than the moderately differentiated group. However, the values between the moderately and poorly differentiated groups were similar. n DWI, apparent diffusion coefficient

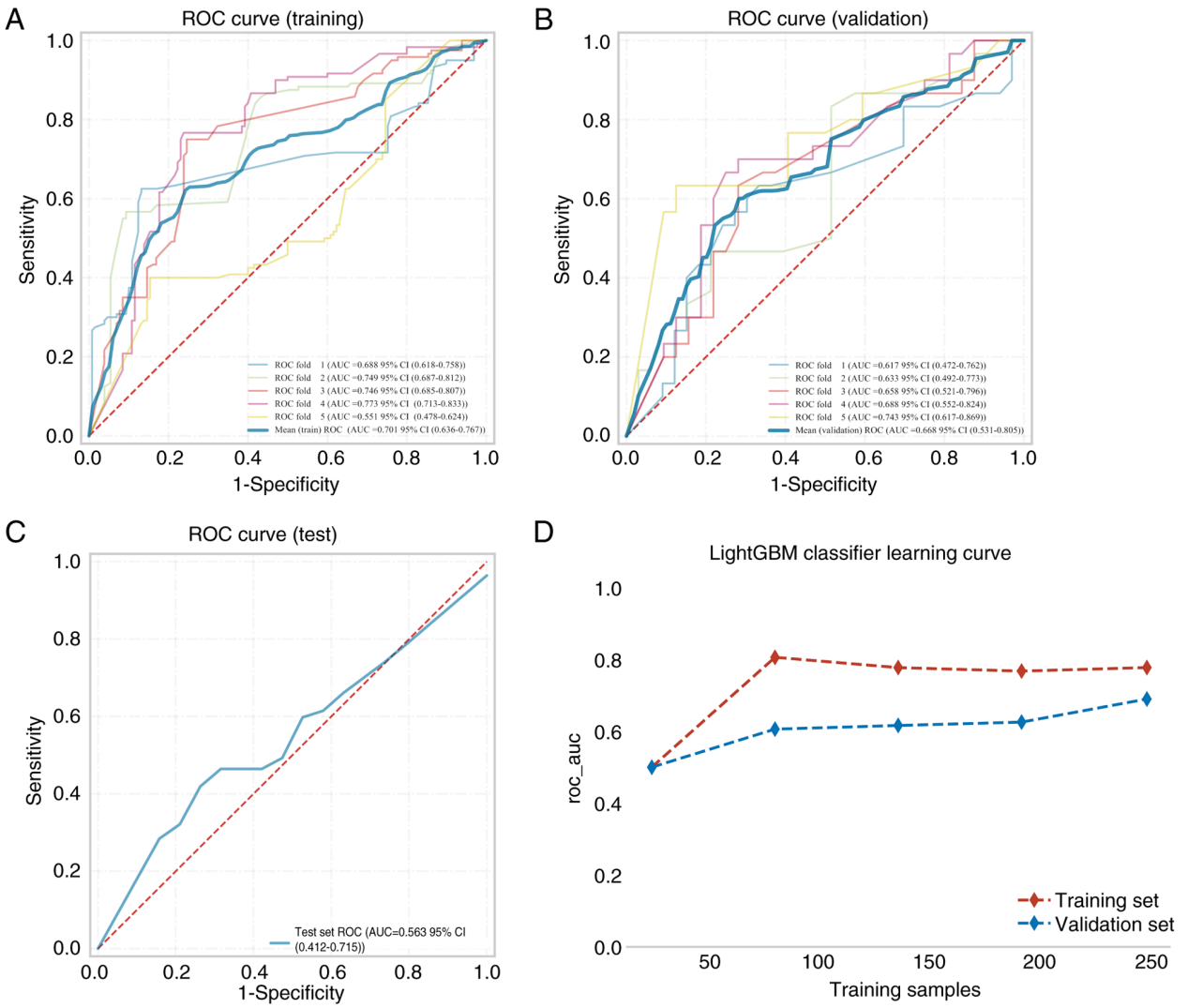

Figure 3. ROC curves of the intratumoral T1-LightGBM model for the training, validation and test groups. ROC curves and AUC values for the (A) training set, (B) validation set and (C) test set. (D) Learning curves. LightGBM, Light Gradient-Boosting Machine; ROC, receiver operating characteristic; AUC, area under the curve; CI, confidence interval.

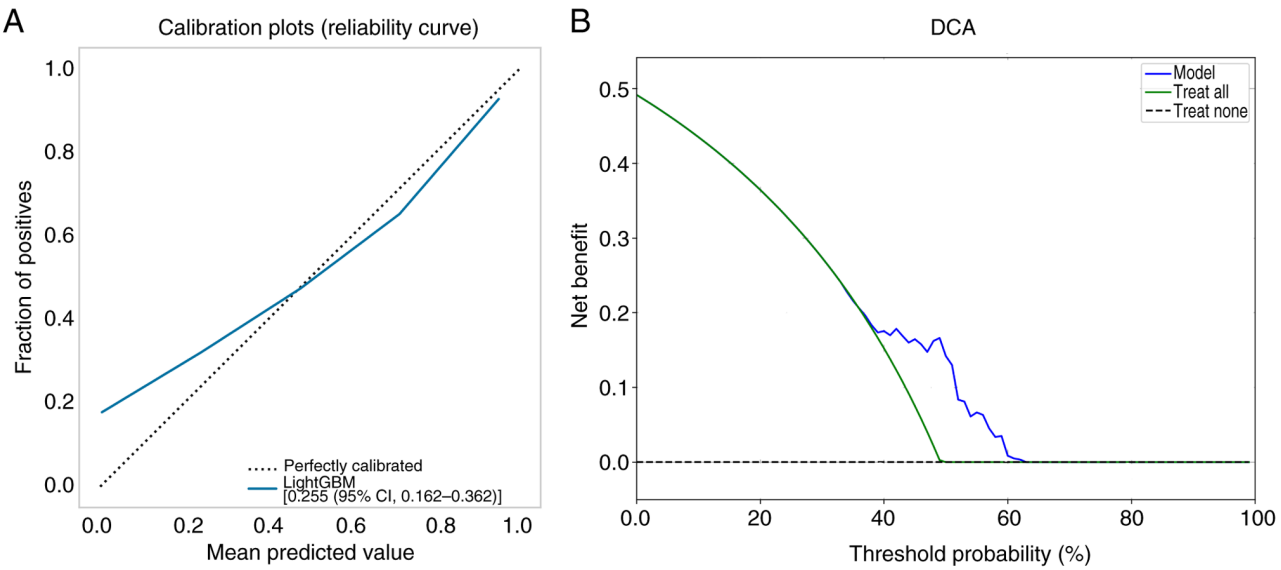

Figure 4. Calibration plots and DCA for the intratumoral + peritumoral 5-mm T1-LightGBMmodel for predicting pathological differentiation. (A) Calibration curve depicts the extent of consistency between the predicted probability and observed probability. (B) DCA of the LightGBM model. DCA, decision curve analysis; LightGBM, Light Gradient-Boosting Machine; CI, confidence interval.

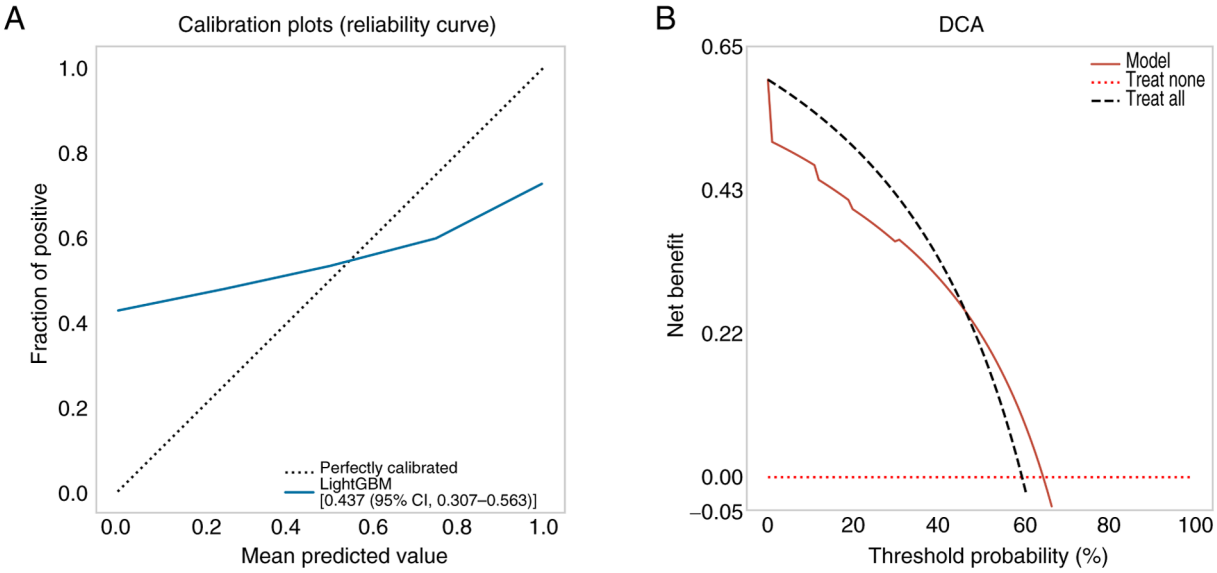

Figure 5. Calibration plots and DCA of the intratumoral T1-LightGBM model for predicting pathological differentiation. (A) Calibration curve depicts the extent of consistency between the predicted probability and observed probability. (B) DCA of the LightGBM model. DCA, decision curve analysis; LightGBM, Light Gradient-Boosting Machine; CI, confidence interval.

(ADC) values have also been used to assess pathological grading. Curvo-Semedo *et al* (40) noted that poorly differentiated tumors tended to exhibit lower ADC values compared with moderately and highly differentiated tumors, although statistical significance was not reached. Zhou *et al* (41) also reported no significant ADC differences within the traditional WHO grading system. However, when adopting the poorly differentiated clusters grading system (42), ADC and intravoxel incoherent motion (IVIM) parameters, such as perfusion fraction f and pseudo-diffusion coefficient D*, demonstrated significant differences between high- and low-grade tumors, with clear correlations between perfusion metrics and tumor grade (r=0.842, P<0.001; and r=0.356, P=0.011). This suggests that IVIM parameters may be valuable for grading. Yuan *et al* (43) further extended the analysis to the peritumoral region and reported that higher peritumoral-to-tumor ADC ratios and ADCp mean values were associated with poor differentiation, T3-4 stage and adverse features such as lymph node metastasis (LNM), extranodal extension, tumor deposits and lymphovascular invasion (LVI). They also reported that the peritumoral-to-tumor ADC ratio outperformed tumor ADC in assessing prognostic factors.

Clinically, treatment strategies for RC are primarily based on TNM staging, which does not fully capture inter-patient heterogeneity within the same stage. Pathological differentiation serves as an important complementary indicator to optimize risk stratification and therapeutic decision-making (44,45). Numerous studies have reported that poor differentiation is associated with higher local recurrence and worse overall survival compared with well differentiation (46,47). Therefore, it is classed as a high-risk feature in the European Society for Medical Oncology and the National Comprehensive Cancer Network (NCCN) guidelines (10). The NCCN and the American Society of Colon and Rectal Surgeons further specify in their local excision criteria for early RC that appropriate candidates should have tumors of <3 cm, well-to-moderately differentiated histology and no LVI (48). Additional studies support incorporating tumor grade into risk assessment. Cho *et al* (49) reported that in pT1 RC and colon cancer, moderate/poor differentiation was significantly associated with LNM (P=0.006 and P=0.002, respectively) and was an independent predictor of LNM (odds ratio, 1.38-8.13; P=0.008). Emile *et al* (50) developed a risk-scoring model integrating tumor grade with nodal stage and reported that, compared with well differentiated rectal adenocarcinoma, poorly differentiated and undifferentiated tumors had a markedly increased risk of LVI (more than threefold). Considering the similar trends observed for moderately and poorly differentiated tumors across functional imaging parameters, and the frequent consideration in clinical guidelines and prior studies that these categories share comparable aggressive biology, the present study combined moderately and poorly differentiated RCs into a 'non-well differentiated' group. This grouping strategy helps clarify gradations of tumor aggressiveness, enhances the ability of the model to identify clinically high-risk patients, and provides more accurate guidance for treatment decisions. For example, in mid-to-low RC initially staged as T3a/b by MRI, if the model predicts moderate/poor differentiation, clinicians may prioritize neoadjuvant chemoradiotherapy over immediate surgery, as the true biological behavior may be more aggressive than suggested by staging alone (51).

In addition to imaging features, studies by Shibutani *et al* (52) and Ryuk *et al* (53) reported that serum CEA and CA 19-9 are independent prognostic factors for RC. Elevated preoperative CEA levels were associated with tumor size and T-stage, whilst high CA19-9 levels were reported to be associated with tumor stage (54). This is consistent with the findings of the present study, in which elevated CA 19-9 levels demonstrated a significant association with poorer

differentiated RC (P=0.014), further supporting the auxiliary value of serum biomarkers in assessing tumor biology. Serum biomarkers reflect systemic tumor burden and metabolic status (55), whereas radiomic features quantify local tumor heterogeneity (24). Their combination could provide multi-dimensional predictive information, enhancing accuracy and clinical utility.

However, the current study has several limitations. First, it adopted a single-center retrospective design which may introduce selection bias, and the sample size was relatively small, particularly for the independent test cohort. More multi-center cohorts are needed for external validation to assess the robustness and reproducibility of the predictive model and to strengthen the conclusions of the present study. Second, radiomics features are sensitive to scanning protocols and equipment parameters. Consequently, standardized image acquisition and feature harmonization should be promoted in the future to improve the generalizability of the model. In addition, tumor region annotation currently relies on manual delineation which may introduce inter-observer variability. Developing automatic or semi-automatic segmentation algorithms is an important direction for improvement. Finally, the current study focused solely on radiomics features. In future work, the plan is to explore integration with clinicopathological indicators and molecular biomarkers, such as genomic and transcriptomic features, to build multi-modal fusion models, enabling more refined patient stratification and further enhancing clinical translational value.

In conclusion, the present study highlights the potential of peritumoral features as a non-invasive tool for predicting RC differentiation. Notably, the integrated model employing the LightGBM algorithm on T1-weighted sequences, which combined both intratumoral and 5-mm peritumoral features, demonstrated promising predictive potential for individualized RC differentiation, thereby contributing to the development of personalized treatment strategies.

Acknowledgements

Not applicable.

Funding

No funding was received.

Availability of data and materials

The data generated in the present study may be requested from the corresponding author.

Authors' contributions

HL collected, analyzed and organized data, and participated in drafting and revising the manuscript. HZ provided supervision, guided the manuscript revision process and assisted in data analysis. QZ performed data collection and operated specialized software. JY contributed to the writing and revision of the article. HL and JY conceived the study and designed the methodology. HL and JY confirm the authenticity of all the raw data. All authors read and approved the final manuscript.

Ethics approval and consent to participate

The present study was performed according to the guidelines of the Declaration of Helsinki and approved by the Medical Ethics Committee of Affiliated Hospital of North Sichuan Medical College (approval no. 2024ER490-1). The requirement for informed consent was waived.

Patient consent for publication

Not applicable.

Competing interests

The authors declare that they have no competing interests.

References

1. Sung H, Ferlay J, Siegel RL, Laversanne M, Soerjomataram I, Jemal A and Bray F: Global cancer statistics 2020: GLOBOCAN estimates of incidence and mortality worldwide for 36 cancers in 185 countries. CA Cancer J Clin 71: 209-249, 2021.
2. Nagtegaal ID, Odze RD, Klimstra D, Paradis V, Rugge M, Schirmacher P, Washington KM, Carneiro F and Cree IA; WHO Classification of Tumours Editorial Board: The 2019 WHO classification of tumours of the digestive system. Histopathology 76: 182-188, 2020.
3. Jiang C, Liu Y, Xu C, Shen Y, Xu Q and Gu L: Pathological features of lymph nodes around inferior mesenteric artery in rectal cancer: A retrospective study. World J Surg Oncol 19: 152, 2021.
4. Junginger T, Goenner U, Hitzler M, Trinh TT, Heintz A, Wollschlaeger D and Blettner M: Long-term oncologic outcome after transanal endoscopic microsurgery for rectal carcinoma. Dis Colon Rectum 59: 8-15, 2016.
5. Garcia-Aguilar J, Renfro LA, Chow OS, Shi Q, Carrero XW, Lynn PB, Thomas CR Jr, Chan E, Cataldo PA, Marcet JE, *et al*: Organ preservation for clinical T2N0 distal rectal cancer using neoadjuvant chemoradiotherapy and local excision (ACOSOG Z6041): Results of an open-label, single-arm, multi-institutional, phase 2 trial. Lancet Oncol 16: 1537-1546, 2015.
6. Glynne-Jones R, Wyrwicz L, Tiret E, Brown G, Rödel C, Cervantes A and Arnold D; ESMO Guidelines Committee: Rectal cancer: ESMO Clinical Practice Guidelines for diagnosis, treatment and follow-up. Ann Oncol 29 (Suppl 4): iv263, 2018.
7. Ueno H, Hase K, Hashiguchi Y, Shimazaki H, Yoshii S, Kudo SE, Tanaka M, Akagi Y, Suto T, Nagata S, *et al*: Novel risk factors for lymph node metastasis in early invasive colorectal cancer: A multi-institution pathology review. J Gastroenterol 49: 1314-1323, 2014.
8. Doornebosch PG, Ferenschild FT, de Wilt JH, Dawson I, Tetteroo GW and de Graaf EJ: Treatment of recurrence after transanal endoscopic microsurgery (TEM) for T1 rectal cancer. Dis Colon Rectum 53: 1234-1239, 2010.
9. Hahnloser D, Wolff BG, Larson DW, Ping J and Nivatvongs S: Immediate radical resection after local excision of rectal cancer: An oncologic compromise? Dis Colon Rectum 48: 429-437, 2005.
10. Fields AC, Lu P, Hu F, Hirji S, Irani J, Bleday R, Melnitchouk N and Goldberg JE: Lymph node positivity in T1/T2 rectal cancer: A word of caution in an era of increased incidence and changing biology for rectal cancer. J Gastrointest Surg 25: 1029-1035, 2021.
11. Horvat N, Carlos Tavares Rocha C, Clemente Oliveira B, Petkovska I and Gollub MJ: MRI of rectal cancer: Tumor staging, imaging techniques, and management. Radiographics 39: 367-387, 2019.
12. Kleiner DE: Hepatocellular carcinoma: Liver biopsy in the balance. Hepatology 68: 13-15, 2018.
13. Song M, Li S, Wang H, Hu K, Wang F, Teng H, Wang Z, Liu J, Jia AY, Cai Y, *et al*: MRI radiomics independent of clinical baseline characteristics and neoadjuvant treatment modalities predicts response to neoadjuvant therapy in rectal cancer. Br J Cancer 127: 249-257, 2022.

14. Ameli S, Venkatesh BA, Shaghaghi M, Ghadimi M, Hazhirkarzar B, Rezvani Habibabadi R, Aliyari Ghasabeh M, Khoshpouri P, Pandey A, Pandey P, *et al*: Role of MRI-derived radiomics features in determining degree of tumor differentiation of hepatocellular carcinoma. Diagnostics (Basel) 12: 2386, 2022.
15. Liu HF, Lu Y, Wang Q, Lu YJ and Xing W: Machine learning-based CEMRI radiomics integrating LI-RADS features achieves optimal evaluation of hepatocellular carcinoma differentiation. J Hepatocell Carcinoma 10: 2103-2115, 2023.
16. Hirata E and Sahai E: Tumor microenvironment and differential responses to therapy. Cold Spring Harb Perspect Med 7: a026781, 2017.
17. Liu HF, Wang M, Wang Q, Lu Y, Lu YJ, Sheng Y, Xing F, Zhang JL, Yu SN and Xing W: Multiparametric MRI-based intratumoral and peritumoral radiomics for predicting the pathological differentiation of hepatocellular carcinoma. Insights Imaging 15: 97, 2024.
18. Park H, Kim KA, Jung JH, Rhie J and Choi SY: MRI features and texture analysis for the early prediction of therapeutic response to neoadjuvant chemoradiotherapy and tumor recurrence of locally advanced rectal cancer. Eur Radiol 30: 4201-4211, 2020.
19. Kim JH, Shin JK, Lee H, Lee DH, Kang JH, Cho KH, Lee YG, Chon K, Baek SS and Park Y: Improving the performance of machine learning models for early warning of harmful algal blooms using an adaptive synthetic sampling method. Water Res 207: 117821, 2021.
20. Khan TM, Xu S, Khan ZG and Uzair Chishti M: Implementing multilabeling, ADASYN, and relieff techniques for classification of breast cancer diagnostic through machine learning: Efficient computer-aided diagnostic system. J Healthc Eng 2021: 5577636, 2021.
21. Bates DDB, Homsi ME, Chang KJ, Lalwani N, Horvat N and Sheedy SP: MRI for rectal cancer: Staging, mrCRM, EMVI, lymph node staging and post-treatment response. Clin Colorectal Cancer 21: 10-18, 2022.
22. Xu F, Hong J and Wu X: An integrative clinical and intra- and peritumoral MRI radiomics nomogram for the preoperative prediction of lymphovascular invasion in rectal cancer. Acad Radiol 32: 3989-4001, 2025.
23. Nayak P, Sinha S, Goda JS, Sahu A, Joshi K, Choudhary OR, Mhatre R, Mummudi N and Agarwal JP: Computerized tomography-based first order tumor texture features in non-small cell lung carcinoma treated with concurrent chemoradiation: A simplistic and potential surrogate imaging marker for survival. J Cancer Res Ther 19: 366-375, 2023.
24. Bernatowicz K, Amat R, Prior O, Frigola J, Ligero M, Grussu F, Zatse C, Serna G, Nuciforo P, Toledo R, *et al*: Radiomics signature for dynamic monitoring of tumor inflamed microenvironment and immunotherapy response prediction. J Immunother Cancer 13: e009140, 2025.
25. Wang X, Dai S, Wang Q, Chai X and Xian J: Investigation of MRI-based radiomics model in differentiation between sinonasal primary lymphomas and squamous cell carcinomas. Jpn J Radiol 39: 755-762, 2021.
26. Hanahan D: Hallmarks of cancer: New dimensions. Cancer Discov 12: 31-46, 2022.
27. Zhang L, Yang Y, Wang T, Chen X, Tang M, Deng J, Cai Z and Cui W: Intratumoral and peritumoral MRI-based radiomics prediction of histopathological grade in soft tissue sarcomas: A two-center study. Cancer Imaging 23: 103, 2023.
28. Lin P, Xie W, Li Y, Zhang C, Wu H, Wan H, Gao M, Liang F, Han P, Chen R, *et al*: Intratumoral and peritumoral radiomics of MRIs predicts pathologic complete response to neoadjuvant chemoimmunotherapy in patients with head and neck squamous cell carcinoma. J Immunother Cancer 12: e009616, 2024.
29. Jiang Y, Wang H, Wu J, Chen C, Yuan Q, Huang W, Li T, Xi S, Hu Y, Zhou Z, *et al*: Noninvasive imaging evaluation of tumor immune microenvironment to predict outcomes in gastric cancer. Ann Oncol 31: 760-768, 2020.
30. Pérez-Morales J, Tunali I, Stringfield O, Eschrich SA, Balagurunathan Y, Gillies RJ and Schabath MB: Peritumoral and intratumoral radiomic features predict survival outcomes among patients diagnosed in lung cancer screening. Sci Rep 10: 10528, 2020.
31. Li Y, Wang P, Xu J, Shi X, Yin T and Teng F: Noninvasive radiomic biomarkers for predicting pseudoprogression and hyperprogression in patients with non-small cell lung cancer treated with immune checkpoint inhibition. Oncoimmunology 13: 2312628, 2024.
32. Wang X, Wei M, Chen Y, Jia J, Zhang Y, Dai Y, Qin C, Bai G and Chen S: Intratumoral and peritumoral MRI-based radiomics for predicting extrapelvic peritoneal metastasis in epithelial ovarian cancer. Insights Imaging 15: 281, 2024.
33. Barge P, Oevermann A, Maiolini A and Durand A: Machine learning predicts histologic type and grade of canine gliomas based on MRI texture analysis. Vet Radiol Ultrasound 64: 724-732, 2023.
34. Scaife CL and Curley SA: Complication, local recurrence, and survival rates after radiofrequency ablation for hepatic malignancies. Surg Oncol Clin N Am 12: 243-255, 2003.
35. Margonis GA, Sergentanis TN, Ntanasis-Stathopoulos I, Andreatos N, Tzanninis IG, Sasaki K, Psaltopoulou T, Wang J, Buettner S, Papalois AE, *et al*: Impact of surgical margin width on recurrence and overall survival following R0 hepatic resection of colorectal metastases: A systematic review and meta-analysis. Ann Surg 267: 1047-1055, 2018.
36. Tang X, Huang H, Du P, Wang L, Yin H and Xu X: Intratumoral and peritumoral CT-based radiomics strategy reveals distinct subtypes of non-small-cell lung cancer. J Cancer Res Clin Oncol 148: 2247-2260, 2022.
37. Cheng J, Liu J, Yue H, Bai H, Pan Y and Wang J: Prediction of glioma grade using intratumoral and peritumoral radiomic features from multiparametric MRI images. IEEE/ACM Trans Comput Biol Bioinform 19: 1084-1095, 2022.
38. Kim HR, Kim SH and Nam KH: Association between dynamic contrast-enhanced MRI parameters and prognostic factors in patients with primary rectal cancer. Curr Oncol 30: 2543-2554, 2023.
39. Shen FU, Lu J, Chen L, Wang Z and Chen Y: Diagnostic value of dynamic contrast-enhanced magnetic resonance imaging in rectal cancer and its correlation with tumor differentiation. Mol Clin Oncol 4: 500-506, 2016.
40. Curvo-Semedo L, Lambregts DM, Maas M, Beets GL, Caseiro-Alves F and Beets-Tan RG: Diffusion-weighted MRI in rectal cancer: Apparent diffusion coefficient as a potential noninvasive marker of tumor aggressiveness. J Magn Reson Imaging 35: 1365-1371, 2012.
41. Zhou B, Zhou Y, Tang Y, Bao Y, Zou L, Yao Z and Feng X: Intravoxel incoherent motion MRI for rectal cancer: Correlation of diffusion and perfusion characteristics with clinical-pathologic factors. Acta Radiol 64: 898-906, 2023.
42. Barresi V, Reggiani Bonetti L, Branca G, Di Gregorio C, Ponz de Leon M and Tuccari G: Colorectal carcinoma grading by quantifying poorly differentiated cell clusters is more reproducible and provides more robust prognostic information than conventional grading. Virchows Arch 461: 621-628, 2012.
43. Yuan Y, Chen XL, Li ZL, Chen GW, Liu H, Liu YS, Pang MH, Liu SY, Pu H and Li H: The application of apparent diffusion coefficients derived from intratumoral and peritumoral zones for assessing pathologic prognostic factors in rectal cancer. Eur Radiol 32: 5106-5118, 2022.
44. Lou S, Huang Y, Du F, Xue J, Mo G, Li H, Yu Z, Li Y, Wang H, Huang Y, *et al*: Development and validation of a deep learning-based pathomics signature for prognosis and chemotherapy benefits in colorectal cancer: A retrospective multicenter cohort study. Front Immunol 16: 1602909, 2025.
45. Huang YQ, Chen XB, Cui YF, Yang F, Huang SX, Li ZH, Ying YJ, Li SY, Li MH, Gao P, *et al*: Enhanced risk stratification for stage II colorectal cancer using deep learning-based CT classifier and pathological markers to optimize adjuvant therapy decision. Ann Oncol 36: 1178-1189, 2025.
46. Oh SY, Park JY, Yang KM, Jeong SA, Kwon YJ, Jung YT, Ma CH, Yun KW, Yoon KH, Kwak JY and Yu CS: Oncologic outcomes of surgically treated colorectal cancer in octogenarians: A comparative study using inverse probability of treatment weighting (IPTW). BMC Gastroenterol 25: 276, 2025.
47. Yang Y, Xu H, Chen G and Pan Y: Stratified prognostic value of pathological response to preoperative treatment in yp II/III rectal cancer. Front Oncol 11: 795137, 2021.
48. Tjandra JJ, Kilkenny JW, Buie WD, Hyman N, Simmang C, Anthony T, Orsay C, Church J, Otchy D, Cohen J, *et al*: Practice parameters for the management of rectal cancer (revised). Dis Colon Rectum 48: 411-423, 2005.
49. Cho SH, Park BS, Son GM, Kim HS, Kim SJ, Park SB, Choi CW, Kim HW, Shin DH and Yun MS: Differences in factors predicting lymph node metastasis between pT1 rectal cancer and pT1 colon cancer: A retrospective study. Am Surg 89: 5829-5836, 2023.

50. Emile SH, Horesh N, Garoufalia Z, Gefen R, Wignakumar A and Wexner SD: Development and validation of a predictive score for preoperative detection of lymphovascular invasion in rectal cancer. J Surg Oncol 131: 1081-1089, 2025.
51. Keller DS, Berho M, Perez RO, Wexner SD and Chand M: The multidisciplinary management of rectal cancer. Nat Rev Gastroenterol Hepatol 17: 414-429, 2020.
52. Shibutani M, Maeda K, Nagahara H, Ohtani H, Sakurai K, Toyokawa T, Kubo N, Tanaka H, Muguruma K, Ohira M and Hirakawa K: Significance of CEA and CA19-9 combination as a prognostic indicator and for recurrence monitoring in patients with stage II colorectal cancer. Anticancer Res 34: 3753-3758, 2014.
53. Ryuk JP, Choi GS, Park JS, Kim HJ, Park SY, Yoon GS, Jun SH and Kwon YC: Predictive factors and the prognosis of recurrence of colorectal cancer within 2 years after curative resection. Ann Surg Treat Res 86: 143-151, 2014.
54. Wang J, Wang X, Yu F, Chen J, Zhao S, Zhang D, Yu Y, Liu X, Tang H and Peng Z: Combined detection of preoperative serum CEA, CA19-9 and CA242 improve prognostic prediction of surgically treated colorectal cancer patients. Int J Clin Exp Pathol 8: 14853-14863, 2015.
55. Farag CM, Antar R, Akosman S, Ng M and Whalen MJ: What is hemoglobin, albumin, lymphocyte, platelet (HALP) score? A comprehensive literature review of HALP's prognostic ability in different cancer types. Oncotarget 14: 153-172, 2023.